HUNGARIAN JOURNAL OF
INDUSTRY AND CHEMISTRY
HJIC

A FRAMEWORK FOR DEMONSTRATION DEVICES USED IN DISTANCE-LEARNING ENVIRONMENTS

PÉTER DECSI*[1], ÁDÁM BORS[1], PÉTER KOCSOR[2], BÁLINT VÖRÖS[2], BARNABÁS HORVÁTH[2], SÁNDOR GUBA[2], ZOLTÁN GUGOLYA[2], SÁNDOR MESTER[1], AND ISTVÁN SZALAI[1,2]

[1]Institute of Mechatronics Engineering and Research, University of Pannonia, Gasparich Márk u. 18/A, Zalaegerszeg, 8900, HUNGARY
[2]Research Centre for Engineering Sciences, University of Pannonia, Egyetem u. 10, Veszprém, 8200, HUNGARY

Distance-learning has become widespread around the world. Many training areas such as engineering require the acquisition of practical rather than theoretical knowledge. In this paper, a framework is presented in the form of four pilot projects which is used for practical laboratory measurements in a distance-learning environment. Four demonstration devices consisting of an induction motor drivetrain, a magnetorheological clutch as well as a rolling resistance and an ultrasonic sensor were built and several examples of measurements presented. The system, based on accessible and user-friendly hardware, is cost-effective, simple to program and can be adapted to suit any application.

Keywords: distance learning, practice-based learning, demonstration device

1. Introduction

Remote learning provides an effective method for educators and students to remain connected and engage with learning content while working from home. Several tools are available to teach theoretical knowledge, e.g., learning management systems and video conferencing solutions. Since learning can be synchronous or asynchronous, both approaches require different tools.

The efficiency of their usage depends on how prepared the parties involved are. During the COVID-19 pandemic, educational institutions had to start using virtual environments as well as stop on-site education and were unable to provide appropriate practical training for their students. Even though remote learning can be effective, a transition from traditional methods must be made [1].

Although numerous demonstration devices have already been presented [2], few of them are capable of distance learning and many of them are only simulations [3]. Since practical training is based on self-experience, available distance learning tools are insufficient. In this paper, a universal tool is presented for distance practical training in the form of four example projects.

The demonstration devices are suitable for distance learning. The user is connected to a microcomputer through the internet, after an operator grants access to it. It provides attended and unattended access to multiple users simultaneously, offline and cloud connectivity, file transfer as well as instant messaging (chat). The educator is able to monitor the learning path and provide instant feedback to students, which is necessary for its effective use [4].

2. Framework

Access to the front end of the framework is provided by a remote desktop client based on Virtual Network Computing (VNC) technology. The software can be run on multiple platforms; it has versions for Windows, macOS, Linux, iOS, Android, Solaris, HP-UX, and IBM AIX operating systems. The back end of the system runs on a Raspberry Pi microcomputer called the VNC Server.

The graphical user interface (GUI) of the operating system is modified on the server that enables it to be controlled using a touchscreen and remotely simultaneously. The control software of the demonstration device is written in Python which is the most common programming language nowadays. The base of the program is a GUI that uses the Tkinter Python module, moreover, the widgets are designed to be simple and readable [5]. The program is tabbed, the first tabs contain lessons and tutorials about its content. It is possible to embed videos from video sharing sites.

The teaching materials are image files, which can be created from a premade PowerPoint template. The appropriate image size, appearance, font size, etc. is set to look identical and be easily readable on multiple platforms.

*Correspondence: decsi.peter@mk.uni-pannon.hu

Figure 1: Graphical user interface of the presented framework.

Figure 2: Demonstration device of an induction motor drivetrain. One two-pole (2) and one four-pole (3) induction motor were connected with flexible couplings. The motors were driven by frequency converters (8). A small DC motor was used as a tachogenerator (1). The power distribution network and control circuit were placed in a plastic box (4). The Raspberry Pi microcomputer (7) had a separate power supply (6) and was connected to a 7-inch display (5).

The measurements, control algorithms and displays are unique to the type of demonstration device used. Only the GUI elements, e.g. buttons, sliders or labels, are provided for the programmers using the framework. In Fig. 1, the GUI of the induction motor drivetrain is presented.

The control algorithms are written in the Python language and the Integrated Development Environment (IDE) used can be chosen arbitrarily by the programmer, only the necessary Python modules need to be installed. Students can access live videos from the device to see the effects of their actions.

3. Induction motor drivetrain

Induction motors are widely used in industry due to their simple and rugged construction, cost-effectiveness as well as maintenance-free and efficient operation. Their simple and robust construction, reliability and power efficiency also fulfil the challenging requirements of the automotive industry. The key to the application of these motors is the control system. An inverter or variable frequency drive (VFD) controls the frequency and AC voltage to set the rotational speed of the motor. It provides a high starting torque as well as high level of efficiency and offers several options to work as a whole system.

Engineering students in the industry are expected to have an understanding of the working principles of an induction motor. In this demonstration device, two induction motors are mounted on a plate (Fig. 2). One of them is a three-phase two-pole squirrel cage induction motor rated at 200 W, the other is a three-phase four-pole squirrel cage induction motor rated at 120 W. The motors are driven by suitable Omron VS mini J7 VFDs. They are compact general-purpose inverters, which are simple to use as well as have several digital and analogue channels.

The larger motor has a double-sided shaft to which a DC motor is mounted and functions as a tachogenerator that measures the shaft speed, which enables the demonstration of the slip of the motor.

The digital inputs of the inverter are used in this project to enable the rotational direction selectors. The analogue input is a speed reference and the output is a current monitor related to the connected motor. The VFD is set to th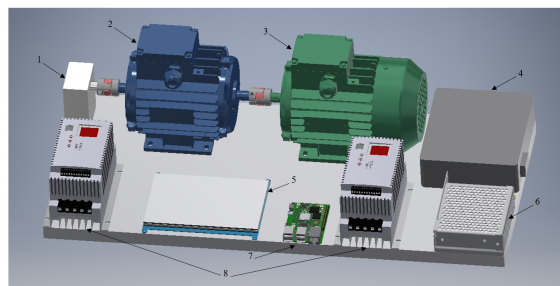e V/f (voltage, frequency control) mode, so the voltage and frequency is set according to the set speed by the analogue input.

An external MCP3008 Analog-to-Digital (A/D) converter and a MCP41010 8-bit digital potentiometer are connected to the Raspberry Pi. The A/D converter is used for the current monitoring and the potentiometer is used to set the reference speed in the VFD. Both integrated circuits communicate through Serial Peripheral Interface (SPI) communication with the microcomputer.

The first three tabs on the program consist of lessons concerning induction motors and VFDs as well as a tutorial for configuring the inverters. Videos are embedded in the fourth tab about induction motors and VFDs. At the time of writing, three measurement tasks are available on this device. One of them is manual control, where tasks written in the provided worksheet can be carried out. Automatic measurement tasks are located in the following two tabs, including a demonstration outlining how an induction motor can be started (Fig. 3) and example measurements of acceleration due to the centre of gravity of the eccentric mass at multiple rotational speeds.
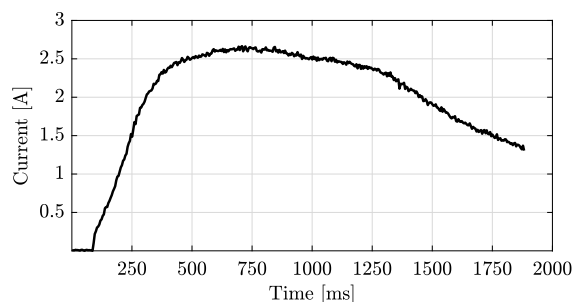

Figure 3: Measurement example of the induction motor drivetrain. The example presents the starting current of the motor as a function of time using frequency converters.
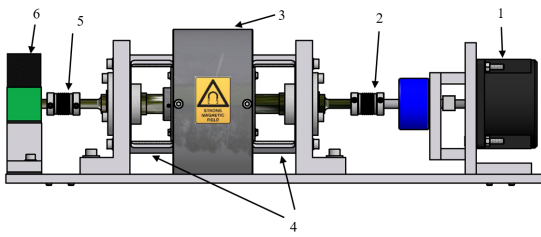
Figure 4: Demonstration device of a magnetorheological clutch. Our magnetorheological device uses an induction motor (1) as a torque source driven by a VFD, moreover, both the driver and driven parts are connected by a flexible coupling (2, 5) to the actual clutch (3). The clutch is held in place by slotted placeholders (4).
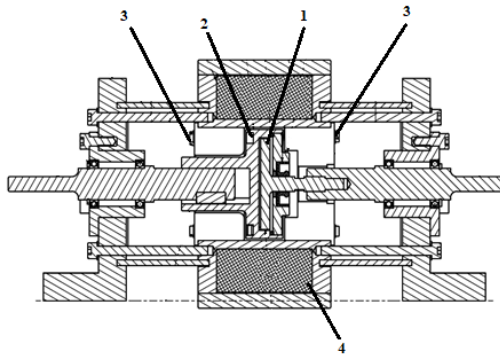

Figure 6: Measurement example of the MR clutch. The transmitted torque of the clutch at a constant speed as a function of the magnetic induction.

Figure 5: Schematic diagram of the magnetorheological clutch. The magnetorheological fluid was located between the input (1) and output (2) disks. The input disk was connected to the shaft by a ball bearing. The clutch was sealed by an O-ring at the output disk and an oil seal at the ball bearing. A coil (4) consisting of approximately 1200 turns of copper wire was located around the disks. The magnetic field lines were directed through the fluid with the help of magnetic flux guiders (4).

4. Magnetorheological clutch

Magnetorheological (MR) fluids are intelligent materials that exhibit the remarkable property of being able to change their rheological properties in the presence of an external magnetic field [6]. They are composed of small ($10\,\mu$m) particles with permeability μ_{p} suspended in a carrier fluid with permeability μ_{f} ($\mu_{\mathrm{f}} < \mu_{\mathrm{p}}$). When a magnetic field is applied to the fluid, the particles acquire a magnetic dipole moment and become arranged in pairs before forming chain-like structures, which act against the shear force producing a change in the apparent viscosity. This phenomenon is used in various applications, namely in brakes [7], clutches [8], superfinishing [9], and dampers [10]. It can be used in clutches to precisely control the transmitted torque by varying the magnetic field. Magnetorheological clutches can be disk-type or cylindrical. For our demonstration, the disk-type MR clutch depicted in Fig. 4 was developed and built.

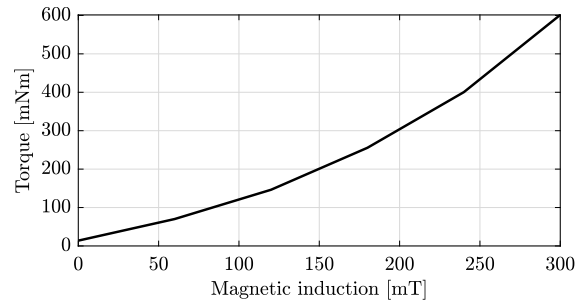The transmitted static torque was measured indirectly by a strain gauge connected to a HX711 ADC (Analogue-to-Digital Converter). Using the known force, the acting distance torque could be calculated. The induction motor was driven by a frequency converter and the coil excited by pulse-width modulation (PWM). A cross-section of the clutch can be seen in Fig. 5. The clutch can transmit approximately $0.6\,\mathrm{Nm}$ of torque at its maximum magnetic induction of $80\,\mathrm{mT}$.

Students can measure the torque in the form of a graph as both a function of the magnetic field Fig. 6 and rotational speed using the provided sliders and displays.

5. Equipment used to measure the rolling resistance coefficient

The rolling resistance force and rolling resistance coefficient (RRC) play important roles in the automotive industry, because they are physical constants that describe the interaction between the road surface and tyres. The rolling friction is a driving resistance force that motor vehicles are subjected to which influences several parameters, including fuel consumption. The goal was to design and implement a piece of experimental equipment for demonstration purposes to measure the coefficient of rolling friction on different modelled road surfaces. The drum arrangement for measuring was chosen, which is widespread in the industry and occupies little space [11].

The measuring equipment consisted of a drum with a large diameter, which represented the modelled road surface, that was rotated by an AC induction motor; a test wheel, which was moved by linear stages; and a frame, which held the parts of the equipment together. Although the road surfaces, composed of rubber, textile and a foam-like material, were adhered to the surface of the drum, it was possible to change them.

A CAD model of the measuring equipment is shown in Fig. 7. The RRC was measured based on the measurement of the rolling resistance force. Since the rolling resistance is a force, this is the most direct method of measuring it. The rolling resistance acts on the connection point between the wheel and drum. Even though the line of action is vertical, its direction depends on the direction of rotation.

The apparatus measured the force using load cells rotated in both clockwise and anticlockwise directions be-
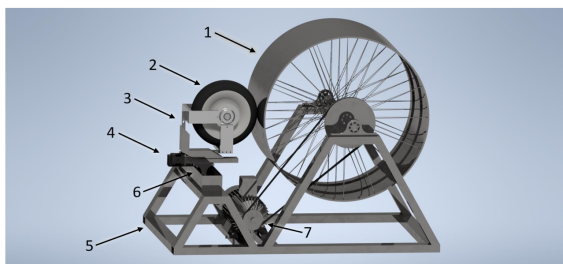
Figure 7: The CAD model of the apparatus: 1. drum using different modelled road surfaces, 2. test wheel, 3. test wheel mounted on load cells, 4. linear stage for moving the test wheel towards the drum, 5. frame, 6. linear stage for lowering the test wheel onto different surfaces, 7. AC motor driving the drum.
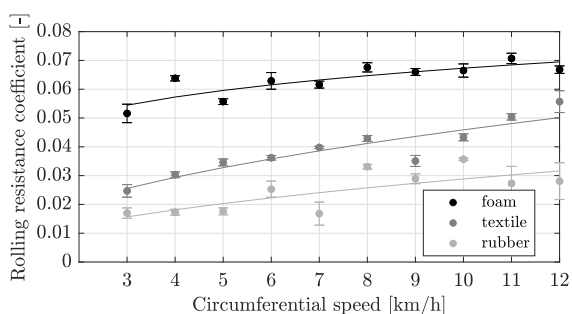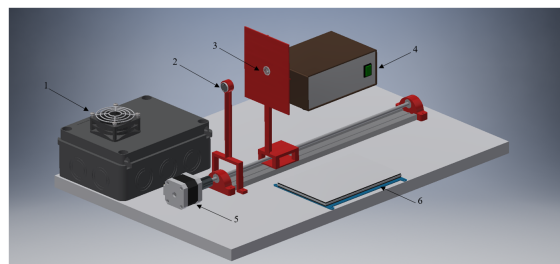

Figure 9: Measuring the ultrasonic distance. The device consisted of a fixed ultrasonic transmitter (2) and a receiver (3) moved by a linear stage driven by a stepper motor (5). The control system and circuit (1) as well as the power distribution and power supply system (4) were located in separate boxes. A 7-inch display was installed on the device (6).
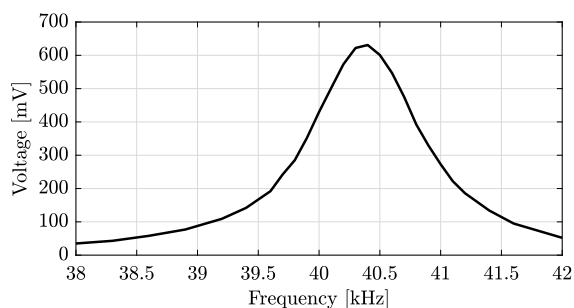

Figure 8: The rolling resistance coefficient measured on the three modelled road surfaces.

Figure 10: Example measurement made by the ultrasonic sensor demonstration device. The example shows the resonance curves of both the transmitter and receiver.

fore calculating the coefficient according to the difference between the two results. On a graphical user interface, the user can select the road surface to be modelled as well as the compressive force between the test wheel and drum. Each measurement is also presented on this graphical user interface.

Several test measurements were made using different settings and the repeatability of each measurement investigated. The RRCs on the different road surfaces are easily distinguishable and the relative standard deviations acceptable (smaller than 20%) for demonstration purposes. Although no values for these modelled road surfaces are found in the literature, the measured coefficients correspond to values measured of tyres on asphalt and dirt roads.

The dependence of the RRC on the circumferential speed, which varied between $3\,\mathrm{km/h}$ and $12\,\mathrm{km/h}$, was investigated. Measurements on all three modelled road surfaces were made using the same parameters ($20\,\mathrm{N}$ compressive force and $0.8\,\mathrm{bar(g)}$ tyre pressure). The results with descriptive statistics are shown in Fig. 8. The RRC increases proportionally to the circumferential speed as expected and is in agreement with the literature [12].

6. Ultrasonic distance measurements made by a sensor

Ultrasound are high-frequency sound waves ranging from $20\,\mathrm{kHz}$ to a few MHz that cannot be detected by the hu-

man ear. Ultrasound can be produced by piezoelectric crystals since when an AC voltage is applied across the crystals, mechanical displacement occurs. By choosing the appropriate degree of excitation, piezoelectric crystals may even exhibit ultrasonic emission. Piezoelectric crystals are polarized by mechanical deformation and the voltage can be measured between opposite plates of a crystal. As a result of vibrations (e.g., ultrasound), an alternating voltage can be measured between the opposite plates of a crystal at the same frequency as the vibrational frequency, i.e., these crystals can also act as an ultrasound receiver.

The measuring arrangement consisted of an ultrasonic transmitter and an ultrasonic receiver (Fig. 9). The distance between the transmitter and receiver could be set using a linear stage. Since the ultrasonic transmitter was driven by a PWM (Pulse-width modulation) signal, the fill factor and frequency of which could be changed, the device was suitable for two measurement tasks.

One of the measurement tasks was measuring the resonance curve (Fig. 10). The algorithm set the distance between the transmitter and receiver at $60\,\mathrm{mm}$. By changing the frequency of the ultrasound emitted by the transmitter using a slider on the user interface, the resonance curve of the receiver could be determined. The amplitude of the receiver signal could be read on a pop-up window. By plotting the amplitudes as a function of frequency, both

the resonance curve and resonance frequency could be measured. The frequency could be set between $38\,\text{kHz}$ and $42\,\text{kHz}$.

The other measurement task measured the amplitude of the voltage at the receiver as a function of the distance between the transmitter and receiver at the resonance frequency determined by the previous task. The distance could be set between $10\,\text{mm}$ and $300\,\text{mm}$.

7. Summary

A framework for a demonstration device has been presented by four pilot projects which is capable of providing practical knowledge in distance learning environments. Since the device can connect to the Internet, students are able to complete tasks set by the educator remotely. The framework is user-friendly for both programmers and users. Only authorized persons are allowed to access the device, which also provides real-time monitoring and feedback for the educators. The framework is easily adaptable to many applications.

Acknowledgement

REFERENCES

[1] UNESCO IEASALC: COVID-19 and higher education: Today and tomorrow, Tech. Rep., UNESCO, 2020, http://www.guninetwork.org

[2] Perea Martins, J.E.: An educational software for measurements demonstrations and data logging with Arduino boards, *Phys. Educ.*, 2020, **55**(6), 063004 DOI: 10.1088/1361-6552/abae25

[3] La Rocca, P., Riggi, F., Pinto, C.: Remotely teaching Arduino by means of an online simulator, *Phys. Educ.*, 2020, **55**(6), 063003 DOI: 10.1088/1361-6552/abaa21

[4] Wilson, G., Stacey, E.: Online interaction impacts on learning: Teaching the teachers to teach online, *Australas. J. Educ. Technol.*, 2004, **20**(1), 106675 DOI: 10.14742/ajet.1366

[5] Richardson, R.T., Drexler, T.L., Delparte, D.M.: Color and Contrast in E-Learning Design: A Review of the Literature and Recommendations for Instructional Designers and Web Developers, Tech. Rep.,**10**(4), 2014 https://jolt.merlot.org/vol10no4/Richardson_1214.pdf

[6] Rankin, P.J., Ginder, J.M., Klingenberg, D.J.: Electro- and magneto-rheology, *Curr. Opin. Colloid Interface Sci.*, 1998, **3**(4), 373–381 DOI: 10.1016/S1359-0294(98)80052-6

[7] Li, W.H., Du, H.: Design and experimental evaluation of a magnetorheological brake, *Int. J. Adv. Manuf. Technol.*, 2003, **21**(7), 508–515 DOI: 10.1007/s001700300060

[8] Latha, K.H., Usha Sri, P., Seetharamaiah, N., Assistant, S.: Design and Manufacturing Aspects of Magneto-rheological Fluid (MRF) Clutch, *Mater. Today: Proc.*, 2017, **4**(4), 1525–1534 DOI: 10.1016/j.matpr.2017.01.175

[9] Jang, K.I., Seok, J., Min, B.K., Jo Lee, S.: An electrochemomechanical polishing process using magnetorheological fluid, *Int. J. Mach. Tool. Manu.*, 2010, **50**(10), 869–881 DOI: 10.1016/j.ijmachtools.2010.06.004

[10] Guan, X.C., Guo, P.F., Ou, J.P.: Modeling and analyzing of hysteresis behavior of magneto rheological dampers, *Procedia Eng.*, 2011, **14**, 2756–2764 DOI: 10.1016/j.proeng.2011.07.347

[11] Andersen, L.G., Larsen, J.K., Fraser, E.S., Schmidt, B., Dyre, J.C.: Rolling Resistance Measurement and Model Development, *J. Transp. Eng.*, 2015, **141**(2), 04014075 DOI: 10.1061/(ASCE)TE.1943-5436.0000673

[12] Ehsani, M., Gao, Y., Gay, S.E., Emadi, A.: Modern Electric, Hybrid Electric, and Fuel Cell Vehicles (CRC Press), 2004 DOI: 10.1201/9781420037739